Towards beyond 1GHz NMR: mechanism of the long-term drift of screening current-induced magnetic field in a Bi-2223 coil

Y. Koyama[1,2], T. Takao[2], Y. Yanagisawa[1,3], H. Nakagome[3], M. Hamada[4], T. Kiyoshi,[5]

M. Takahashi[1,6] and H. Maeda[1,6]

[1]Systems and Structural Biology Center, RIKEN, Yokohama, Kanagawa, 230-0045, Japan.

[2]Sophia University, Yotsuya, Tokyo, 102-8554, Japan.

[3]Faculty of Engineering, Chiba University; Chiba, 236-8522, Japan.

[4] Kobe Steel, Ltd., Kobe, Hyogo, 651-2271, Japan.

[5]Superconducting Materials Center, National Institute for Materials Science, Tsukuba, Ibaraki, 305-0003, Japan.

[6]Graduate School of Yokohama City University, Yokohama, Kanagawa, 230-0045, Japan.

Corresponding author:

Name: Hideaki Maeda

Phone: +81-045-508-7211

Fax: +81-045-508-7360

E-mail address: maeda@jota.gsc.riken.jp

Address: Systems and Structural Biology Center, RIKEN, Yokohama, Kanagawa, 230-0045, Japan.

Abstract

The screening current-induced magnetic field in the $(Bi,Pb)_2Sr_2Ca_2Cu_3O_x$(Bi-2223) insert coil proposed for a beyond 1GHz nuclear magnetic resonance (NMR) spectrometer may generate a long term field drift, resulting in a loss of field-frequency lock operation and an inability to make high resolution NMR measurements. The measured screening current-induced magnetic field of a Bi-2223 double-pancake coil exhibits a hysteresis effect at 4.2K that is reproduced by a numerical simulation based on a finite thickness rectangular superconductor bar model. The screening current-induced field at the coil center is of opposite polarity to that generated by the coil current, and thus the apparent field intensity shows a positive drift with time. On the contrary, the field at a coil end is of the same polarity as the coil field, and the apparent field intensity decreases with time. If we wait for ~1000hr after coil excitation, the field-drift rate approaches the field decay rate of the persistent current of 10^{-8}/hr, suitable for a long-term NMR measurement in a beyond 1GHz NMR spectrometer.

Keywords:

Superconducting magnet, NMR, Bi-2223, beyond 1GHz NMR, Field stability, Screening-current induced magnetic field, Hysteresis, Relaxation, Remanent magnetic field.

1. Introduction

Because of their improved resolution and sensitivity for the nuclear magnetic resonance (NMR) of proteins [1,2] and quadrupole nuclei [3], a large number of 900MHz (21.1T)-class NMR spectrometers have already been installed [4]. Although the magnetic fields of NMR spectrometers have reached as high as 950MHz (22.3T) [5], 1GHz (23.5T) is still the upper limit. However, the use of a high-temperature superconductor (HTS) high field insert should make operation, beyond 1GHz possible. Thus, we have commenced a project to develop a beyond 1GHz NMR spectrometer with an HTS insert [6]; the low-temperature superconductor (LTS) Nb_3Sn innermost coil of the 920 MHz NMR magnet installed in the National Institute for Materials Science (NIMS) in Japan is to be replaced by an $(Bi,Pb)_2Sr_2Ca_2Cu_3O_x$ (Bi-2223) HTS coil and is planned to be operational in NIMS in 2011.

The LTS NMR magnet is usually operated in a persistent current mode and the persistent current decay is $<10^{-8}$/hr. It can be further stabilized to 10^{-10}/hr by a field-frequency lock system installed on the NMR spectrometer [7] which continuously detects ^2H NMR spectra in a sample solution and compensates for persistent field decay and field fluctuations.

Due to the low n-index of the tape used in a Bi-2223 coil and the difficulty in

guaranteeing a superconducting joint, an HTS insert is unlikely to provide a persistent current sufficient for NMR. Therefore, an external DC current supply must continuously provide current [6]; i.e. the coil is operated in driven mode. We described in a previous paper that the field-frequency lock system stabilizes a field fluctuation appearing in driven mode for a 500MHz LTS NMR [7]. However, if the field drift exceeds $3x10^{-6}_{pp}$ ($3ppm_{pp}$), the NMR spectrometer loses lock operation and precise NMR measurement is unachievable; thus, it is necessary to suppress the field fluctuation and the field drift to $<3x10^{-6}_{pp}$ ($3ppm_{pp}$).

Hahn et al. [8] demonstrated that the screening current-induced magnetic field in the Bi-2223 tape generates a remanent magnetic field in a 700MHz low temperature superconductor/ high temperature superconductor (LTS/HTS) NMR. A remanent field was also reported by Gu et al. [9], which was explained by a "finite thickness rectangular bar model" of the flux penetration.[10] Hemmi et al. [11, 12] reported a drift with time of the screening current-induced magnetic field. Recently, Amemiya and Akachi [13] conducted a general kind of numerical simulation on the steady state screening current-induced magnetic field for a 1.3 GHz NMR design. If the long-term field drift due to the screening current-induced magnetic field in a Bi-2223 insert for our beyond 1GHz NMR exceeds $3x10^{-6}_{pp}$/hr ($3ppm_{pp}$/hr), the field-frequency lock system

operates for less than one hour and high resolution NMR is improbable. If we wish to achieve a long term high resolution NMR measurement, the rate of change in the screening current-induced magnetic field required has to be as small as the persistent current decay of 10^{-8}/hr (0.01ppm/hr).

The objective of this paper is to investigate the basic mechanism of the magnetic field drift with time due to the screening current-induced magnetic field, in particular, the connection to the hysteresis effect of flux penetration in a Bi-2223 tape. A numerical simulation based on a finite thickness rectangular superconductor bar model explains these results. Finally, we will discuss the possibility to achieve a field stability of 10^{-8}/hr (0.01ppm/hr) for the beyond 1GHz NMR that includes a Bi-2223 insert coil.

2. Numerical simulation method of the screening current-induced magnetic field

The screening current-induced magnetic field in the Bi-2223 tape is numerically simulated as follows:

(a) The magnetic field distribution for a given coil current is calculated by a finite element method. The model is axisymmetric with the magnetic vector potential as a variable.

(b) A pancake winding is modeled as a set of superconducting concentric rings as shown

in Figure 1 (a), each of which has a thickness of 0.24mm. Considering the aspect ratio of the Bi-2223 tape, we calculate only the azimuthal component of the screening current induced by the radial component of the applied magnetic field. The screening current is calculated based on a finite thickness rectangular superconductor bar model proposed by Brandt [10]; he derived a lens-shaped flux penetration pattern into a rectangular thin superconductor bar, as seen in Fig. 1(b), and demonstrated that the field of full penetration for the tape conductor is one-tenth of the value estimated by the slab model.

$$x_0 = \frac{a}{\cosh\left(\frac{\pi B_a}{J_c \mu_0 d}\right)}, \qquad (1)$$

The position of the flux penetration front x_0 (see Figure 1 (b)) is given by [10] where $2a$ is the tape width, d is the tape thickness, J_c is the critical current density, B_a is the applied perpendicular magnetic field and μ_0 is the magnetic permeability of vacuum. Brandt assumed a superconductor rectangular bar [10], while a multi-filamentary Bi-2223 tape was used in this experiment. The overall critical current density for the Bi-2223 tape was employed for J_c in Eq. (1). The sheet current of the superconducting tape, J_s, which equals to the current for a unit width of the tape, is [10]

$$|J_s| = \frac{2J_c d}{\pi} \arctan\left[\left(\frac{a^2 - x_0^{\,2}}{x_0^{\,2} - x^2}\right)^{0.5} \frac{x}{a}\right] \qquad 0 \le x \le x_0, \quad (2)$$

$$|J_s| = J_c d \qquad x_0 \le x \le a, \quad (3)$$

where x is the distance from the center seen in Fig. 1(b). Integration of the sheet current along x for one half of the ring gives the current for the ring; the sum of the current over all turns on a pancake gives an overall screening current for the pancake, i_{pc}. The pancake is then modeled as a one-turn coil with a current of $+i_{pc}$ for one half and $-i_{pc}$ for another. When the coil is discharged, the opposite-polarity screening current penetrates from the outer surface of the conductor, as seen in Fig. 1(c), which generates a corresponding screening current.

(c) Finally, the magnetic field generated by each pancake is calculated with Biot-Savart's law, which is summed to give the screening current-induced magnetic field strength.

3. Experimental procedure

3.1 Physical parameters of a Bi-2223 coil

A test coil consists of 19 pancakes wound with a multi-filamentary Bi-2223 tape (Sumitomo Electric). The coil is 75mm in inner diameter, 104mm in outer diameter, and

168mm in length. The Bi-2223 tape is 4.1mmx0.22mm and the overall critical current density at 77K is about 90A/mm^2, with silver matrix to superconductor ratio of 1.5. The number of turns is 1634 and the length of the conductor is 459m. The Bi-2223 tape was co-wound with a prepreg fiber-reinforced plastic(FRP) tape, which was then heat treated to harden it. The double-pancakes were stacked together and pressed from the top. The coil inductance was 0.077H. The central magnetic field generated by a unit current in the coil is 109.3G/A. The overall critical current densities for parallel and perpendicular fields are shown in Fig. 2 as a function of the magnetic field; the coil load line is indicated by the dashed line. The maximum attainable current density is 400A/mm^2, corresponding to a coil current of 387A. The magnet is operated at 4.2K.

3.2 Instrumentation and coil charging experiment

Both the axial component of the magnetic field at the coil center, z=0, and at the coil end, z=90mm, were measured by cryogenic Hall sensors (BHT921, F. W. Bell). The coil current from the external current supply was measured by a current transducer (Ultrastab 867-4001, Danfysik). The stability of the DC power supply was ~10^{-5}. Carbon-glass resistors were mounted on the top and bottom of the coil. The magnetic field, coil current, coil temperatures and liquid helium level were recorded every 6 sec.

Details of the cyclic charging and discharging experiments on the coil are described in Section 4. After these cyclic tests, the current supply was disconnected and the remanent magnetic field was measured over a period of 60hr.

4. Results and discussion

4.1 Hysteresis effect and relaxation of the screening current-induced magnetic field

Figure 3 shows the apparent magnetic field measured at the coil center, indicated by the closed circles, and that measured at the coil end, indicated by the open circles, as a function of the coil current; the arrows indicate the charge and discharge of the coil. A hysteresis effect is evident, which is due to the additional screening current-induced magnetic field appearing in the Bi-2223 tape.

Subtraction of the magnetic field generated by the coil current from the apparent field seen in Fig. 3 gives the screening current-induced magnetic field. The open circles in Figure 4 (a) shows the screening current-induced field thus obtained at the coil center, B_{cs} as a function of coil current, while Fig. 4(b) similarly shows the screening current-induced field at the coil end, B_{es}. These changes are summarized as follows:

(1) When the coil is charged from 0A (point O) to +100A (point A), the B_{cs} increases with the coil current in the negative direction, while the B_{es} increases in the positive

direction; they tend to saturate at -198G for B_{cs} and at 192G for B_{es}. Then, when the coil is discharged from 100A (point A) to 0A (point B), the B_{cs} decreases until passing through zero at 50 A and then it increases again in the positive direction along AB. Similar behavior is apparent for the B_{es}, while the field polarity is opposite. Even when they reach the point B, there remains a remanent field of +112G at the coil center and -94G at the coil end.

(2) Current polarity is then reversed and the coil is charged from 0A (point B) to -100A (point C). Both B_{cs} and B_{es} appear to saturate along BC; the saturation value at point C is 158G for B_{cs} and -109G for B_{es}. When the coil is discharged, B_{cs} falls until crossing zero at 60A, and then it increases in the negative direction along CD. Similar behavior is observed for B_{es}, although the field polarity is opposite. The residual magnetic field at point D is -137G for B_{cs} and 144G for B_{es}.

(3) Current polarity is finally reversed again and the coil is charged from 0A (point D) to +100A (point E). Both B_{cs} and B_{es} tend to saturate along DE. While the coil is discharged, both B_{cs} and B_{es} move along EF which coincides with the previous locus of AB.

The numerical simulation results based on finite-thickness rectangular superconductor bar model are indicated by the solid lines in Fig. 4(a) and Fig. 4(b); the

overall critical current density J_c assumed in Eq. (2) and Eq. (3) is 150A/mm^2. The simulation results agree quite well with the experimental results. The hysteresis behavior seen in Fig. 4(a) and (b) is explained based on these simulations by the following arguments. As the current increases from point O to point A, the radial field component gradually penetrates into the conductor from the outer boundary, during which a lens-shaped shielded core is formed apparent in Fig. 1(b). As the flux front approaches the center of the conductor's width, the screening current tends to saturate, resulting in a saturation tendency in the screening current-induced field. When the coil is discharged, an opposite polarity screening current penetrates from the outer boundary, as seen in Fig. 1(c), and thus the screening current-induced field begins to decrease along AB. After theses curves cross zero field, the outer screening current becomes dominant and the screening current-induced field increases again in the opposite direction. The remanent magnetic field at point B is caused by the remaining screening current visible in Fig. 1(c). The solid lines BC, CD, DE and EF are explained similarly.

The flux penetration ratio, defined as $1\text{-}x_0/a$, at +100A is numerically simulated and shown by color coding over the coil cross section in Fig. 5; in the case of full flux penetration, the ratio is 1.0 and it is indicated by red; the ratio is 0 for zero flux penetration and it is shown as blue. For the coil end section, the flux penetration ratio

equals ~1, i.e. flux is fully penetrated. On the contrary, around the coil midplane it is less than 0.5, i.e. flux penetrates less than half of the tape width. Thus, the simulated hysteresis loop for B_{es} saturates at +100A which agrees well with the experimental results. On the other hand, in the case of B_{cs}, the simulated hysteresis loop still increases at 100A, as the flux penetration is incomplete, a situation which is at variance with the experimental results, which shows a saturation tendency.

The drift of the measured magnetic field, at the coil center is shown in Fig. 6 (a), (b) and (c) for +100A, +50A, and -100A respectively, while those at the coil end are shown in Fig. 6(d), (e) and (f) for +100A, +50A and -100A respectively. As the B_{cs} value is negative at +100A, the measured magnetic field at the coil center equals B_{ca}-$|B_{cs}|$, where B_{ca} is the axial field generated by the coil current at the coil center. Fig. 6(a) shows that as B_{cs} is gradually relaxed, the measured magnetic field increases with time. On the contrary, as the B_{es} is positive at +100A, the measured magnetic field at the coil end equals B_{ea}+$|B_{es}|$, where B_{ea} is the axial field generated by the coil current at the coil end. As the B_{es} is relaxed, the magnetic field decreases with time, as seen in Fig. 6(d). When the current sweep was reversed at +100A, the measured magnetic field relaxation rate falls steeply from those obtained at +100A; a similar dependence of the magnetization relaxation rate on the field sweep direction is reported for a

$Y_1Ba_2Cu_3O_x$(YBCO) bulk[14], which will be discussed in the next section. For +50A, both B_{cs} and B_{es} are nearly zero and therefore relaxation of the screening current-induced field is negligible; thus the field remains constant, as seen in Fig. 6(b) and Fig. 6(e). A similar explanation covers the behavior at -100A seen in Fig. 6(c) and Fig. 6(f).

4.2 Basic mechanism of relaxation in remanent magnetic field

The decay of the remanent magnetic field at point F in Fig. 4(b) is shown in Fig. 7. The coil temperature, shown in green(top) and blue(bottom), remains at 4 ~ 5K for an initial time interval of 32hr; the positive remanent field at the coil center, B_{esr}, and the negative remanent field at the coil end, B_{esr}, decrease slowly with time. If the induced screening current flows along the full length(~24m) of conductor on a double pancake and crosses over the silver matrix near both ends of the conductor [15, 16], the outer boundary of the screening current for the remanent field magnetically diffuses from both ends to the center. The magnetic diffusion length over 32hr is 4.8m on each side of the conductor, which is 40% of the half length (12m) of the double pancake conductor; a silver matrix resistivity of $1x10^{-10}\Omega m$ is assumed in this calculation. [17] If this is the case, the remanent field is expected to decay 40% in 33hr. The experimental decay over 33h seen in Fig. 7 is only 3 to 4 G, corresponding to 2 to 3 % of the initial field, and

therefore relaxation is not dominated by magnetic diffusion of the screening current boundary.

If relaxation of the screening current density $J(t)$ is governed by flux creep, the current density changes with time as [18,19]

$$J(t) = J_{c0}\left[1 - \frac{kT}{U_0}\ln\left(\frac{t}{t_0}\right)\right], \qquad (4)$$

where J_{c0} is the critical current density in the absence of thermal activation, t is time, t_0 is the effective flux hopping attempt time, k is Boltzmann's constant, T is the absolute temperature and U_0 is the pinning barrier height in the absence of a Lorentz driving force. If the screening current density vs. time is plotted in a double-logarithmic plot, the slope of the plot corresponds to the normalized relaxation rate, S, which gives the above parameters as follows. [19]

$$S \equiv \frac{d\ln J(t)}{d\ln t} = \frac{1}{J(t)}\frac{dJ(t)}{d\ln t} = -\frac{kT}{U_0} \qquad (5)$$

For the coil end section the flux is fully penetrated and therefore the remanent field $|B_{esr}(t)|$ is proportional to the screening current $J(t)$. The experimental variation of $|B_{esr}|$ vs. time is shown in a double-logarithmic plot in Fig. 8; based on the dashed line, a value for U_0 of 63meV is obtained, which is of the same order as those reported for

Bi2212 single crystal, 17meV at 12K. [20] This data supports the idea that relaxation of the remanent magnetic field is dominated by flux creep.

Amemiya et al. [21] suggested that the HTS filaments in a Bi-2223 tape are partially interconnected. If this is the case, the major part of the screening current flows in a persistent current mode through interconnected filaments and thus its relaxation is dominated by flux creep. The rest current may be quickly dissipated by crossing over to the silver matrix; this might be one of the reasons why the overall critical current density, 150A/mm^2, assumed in the numerical simulation seen in Fig. 4 is smaller than the short sample critical current density(see Fig. 2). We propose that the advanced Bi-2223 tape fabrication processes recently employed to enhance the critical current density, such as the controlled over-pressure sintering method [22], might increase the number of interconnection sites between Bi-2223 filaments, although it may also enhance the critical current density of the Bi-2223 tape conductor.

The interconnection of the Bi-2223 filaments is suppressed if we increase the inter-filament distance of the conductor, or if we use a twisted Bi-2223 tape with an inter-filament resistive barrier [23]; however such a fabrication process simultaneously decreases the critical current density at high fields, which is critical for a high field NMR magnet. If we could further improve a twisted Bi-2223 tape that has a sufficient

critical current density at high fields without possessing interconnection sites, the screening current-induced magnetic field would quickly disappear after changing the magnet field; thus problems such as the hysteresis effect and the long-term field drift shown in this paper, would be solved.

The drop in the relaxation rate of the screen current-induced magnetic fields after reversal of the coil current sweep direction mentioned above has been interpreted as an additional effect of flux creep by Kwasnitza and Widmer [14]; when the coil current sweep direction is reversed at 100A, the magnetic field gradients at the upper and lower ends of the Bi-2223 tape are reversed, acting as barriers for flux entrance into the conductor. The combined effect of this barrier effect and the decrease in net screening current in a tape conductor during discharging the HTS magnet reduces the relaxation rate of the screen current-induced magnetic fields. Further investigations are being made of the barrier effect on the field stability.

For the time interval from t=32hr to 42hr in Fig. 7, $|B_{csr}|$ and $|B_{esr}|$ quickly decrease with time, crossing zero at t=42hr, where the coil temperature is ~110K. Note that temperature coefficient of the offset voltage of the Hall sensor causes a residual offset voltage above this temperature. The value of $|B_{esr}(T)|/|B_{esr}(5K)|$ in this time interval is shown in Fig. 9 as a function of coil temperature, where B_{esr}(T) is the B_{esr} value at

temperature T,, while B_{esr}(5K) is that at 5 K. The dashed line gives the $J_c(T)/J_c$(5K) vs. temperature for the Bi-2223 tape, where J_c(T) is the J_c value at temperature T, while J_c(5K) is that at 5 K. Both curves agree well and it is clear that the decay is due to critical current decay with temperature; we can easily see why the remanent field disappears above 110K, the critical temperature of Bi-2223.

4.3 Discussion towards beyond 1GHz NMR spectrometer

Our beyond 1GHz NMR spectrometer is to be operated in driven mode, due to the difficulty in using persistent current operation. The drift rate of the screening current-induced magnetic field ~5G/ 0.5hr seen above corresponds to $4x10^{-5}$/hr for the 1GHz spectrometer, which is $4x10^{3}$-times larger than the persistent current decay(10^{-8} /hr) for a LTS NMR. A field drift rate of 10^{-8}/hr is necessary for long term field-frequency lock operation, which stabilizes the magnetic field to $<10^{-10}$.[7] Figure 10 shows a double logarithmic plot of $|B_{cs}|$ vs. time at +100A, which seems to follow the flux creep formula seen in Eq. (5); the slope of the plot gives a barrier height of 15meV, which is consistent with those seen in Fig. 8. A linear extrapolation of the dashed line in Fig. 10 suggests that the field drift rate is 2G/hr (corresponding to 10^{-5}/hr for a beyond 1GHz NMR) at t=1hr, while it is three orders of magnitude smaller, about 2mG/hr

(corresponding to 10^{-8}/hr) at t=1000hr. Thus it is probable that if we wait for a sufficiently long time, such as ~1000hr, the positive drift of the central field, due to the relaxation of the screening current-induced magnetic field, slows and reaches the level of the persistent current decay for LTS NMR. This means that a long term high resolution NMR measurement is probably achievable, even if we use a Bi-2223 insert for the spectrometer.

The engineering critical current density required for the beyond 1GHz NMR (>23.5T) insert coil is >300A/mm^2 at 25T. We have decided to use a Bi-2223 tape for this purpose as it is the only mass-produced wire available in sufficient length and with a sufficiently high critical current density, J_c, at high fields [22], and it permits us to use a react-and-wind technique [15] for coil fabrication. Ohkura et al. [24] have already generated a 24.0T magnetic field with a Bi-2223 tape coil in a hybrid magnet.

Both $Bi_2Sr_2CaCu_2O_x$(Bi2212) and YBCO are other candidates for the beyond 1GHz NMR insert coil. Bi2212 has similar levels of engineering critical current density at 25T as Bi2223; Weijers et al.[25] generated a 25.05T field with a Bi2212 tape coil in a resistive backup magnet.[26] If we use an untwisted Bi-2212 tape for the beyond 1GHz NMR, the situation regarding the screening current-induced magnetic field is the same as that for the Bi-2223 tape; however, if we use a powder-in-tube processed

Bi-2212 round wire [27-29] which is sufficiently twisted, the screening current will be reduced quickly due to filament twisting and the effect of screening current-induced magnetic field is negligible.

Recently, Hazelton et al. [30] generated a 26.8T field using a YBCO double-pancake coil with a resistive magnet. A YBCO tape has a superconducting thin layer on the surface and its engineering critical current density is near that of Bi-2223 tape at 25T [31]. For a YBCO tape coil, the screening current flows in the YBCO surface layer of the tape, on the contrary for a Bi2223 tape coil it flows in the interconnected-filament network. Therefore, the intensity of the screening current–induced magnetic field for YBCO coil is several times larger than that for the Bi-2223 coil; as the flux creep activation energy for YBCO is close to that of Bi2223 [20], its relaxation rate should be similar to that of the Bi-2223 coil. If the YBCO layer is divided into stripes along its length [32], the screening current-induced magnetic field will decrease due to decay of the coupling current, resulting in a smaller screening current-induced decoupled magnetic field.

5. Conclusion

(1) The screening current-induced magnetic field for a Bi-2223 coil exhibits a hysteresis

effect; the changes in the magnetic field agree with a numerical simulation based on the finite thickness rectangular superconductor bar model.

(2) The screening current-induced magnetic field drifts with time; if it is of the same polarity as the field generated by the coil current, the apparent magnetic field decreases with time, while if it is of the opposite polarity, the apparent magnetic field increases with time. The central field of the Bi-2223 coil belongs to the latter case.

(3) Based on the drift of the remanent field, we have demonstrated that major part of the screening current flows in persistent current mode through the interconnected-filaments of Bi-2223 and its relaxation is governed by a flux creep process.

(4) The remanent field drops with temperature; it is governed by the temperature dependence of the critical current density of a Bi-2223 tape.

(5) If we wait for a long time, such as ~1000hr, after coil excitation, the field drift due to screening current-induced magnetic field approaches the field decay rate of the persistent current for a LTS NMR, 10^{-8}/hr. Therefore, it is suggested we can achieve a long term NMR measurement, even if we use a Bi-2223 insert for the beyond 1GHz NMR spectrometer.

Acknowledgement

This work is supported by SENTAN, JST in Japan.

References

[1] K. Pervushin, R. Riek, G. Wider and K. Wüthrich, Attenuated T_2 relaxation by mutual cancellation of dipole-dipole coupling and chemical shift anisotropy indicates an avenue to structures of very large biological macromolecules in solution, Proc. Natl. Acad. Sci. USA, **94**, 1997, 12366-12371

[2] R. Riek, G. Wider, K. Pervushin, and K. Wüthrich, Polarization transfer by cross-correlated relaxation in solution NMR with very large molecules, Proc. Natl. Acad. Sci. USA, **96**, 1999, 4918-4923.

[3] Z. Gan, P. Gor'kov, T. A. Cross, A. Samson, and Dominique Massiot, Seeking higher resolution and sensitivity for NMR of quadrupolar nuclei at ultra high magnetic fields, J. Am. Chem. Soc., **124**, 2002, 5634-5635.

[4] T. Kiyoshi, H. Maeda, J. Kikuchi, Y. Ito, H. Hirota, S.i Yokoyama, S. Ito, T. Miki, M. Hamada, O. Ozaki, S. Hayashi, N. Kurihara, H. Suematsu, M. Yoshikawa, S. Matsumoto, A. Sato, and H. Wada, Present Status of 920MHz High Resolution NMR spectroscopy, IEEE Trans. Appl. Supercond.,**14**, 2004, 1608-1612.

[5] A. Twin, J. Brown, F. Domptail, R. Bateman, R. Harrison, M. Lakrimi, Z. Melhem, P. Noonan, M. Field, S. Hong, K. Marken, H. Miao, J. Parrell and Y. Zhang, Present and future applications for advanced superconducting materials in high field

magnets, IEEE Trans. on Appl. Supercond., **17**, 2007, 2295-2298.

[6] T. Kiyoshi, A. Otsuka, S. Choi, S. Matsumoto, K. Zaitsu, T. Hase, M. Hamada, M. Hosono, M. Takahashi, T. Yamazaki, and H. Maeda, NMR Upgrading Project towards 1.05GHz, IEEE Trans. Appl. Supercond., **18**, 2008, 860-863.

[7] Y. Yanagisawa, H. Nakagome, M. Hoshino, M. Hamada, T. Kiyoshi, F. Hobo, M. Takahashi, T. Yamazaki, and H. Maeda, Towards beyond-1GHz solution NMR: internal 2H lock operation in an external current mode, J. Mag. Res. **192**, 2008, 329-337.

[8] S. Hahn, J. Bascunan, W. Kim, E. S. Bobrov, H. Lee, and Y. Iwasa, Field mapping, NMR lineshape, and screening current induced field analyses for homogeneity improvement in LTS/HTS NMR magnets, IEEE Trans. Appl. Supercond. **18**, 2008, 856-859.

[9] C. Gu, T. Qu, and Z. Han, Measurement and calculation of residual magnetic field in a Bi-2223/Ag magnet, IEEE Trans. Appl. Supercond., **17**, 2007, 2394-2397.

[10] E. H. Brandt, Superconductors of finite thickness in a perpendicular magnetic field: strip and slap, Phys. Rev. B **54**, 1996, 4246-4264.

[11] T. Hemmi, N. Yanagi, G. Bansai, K. Seo, K. Takahashi, and T. Mito, Elevtromagnetic behavior of HTS coils in persistent current operation, Fusion Eng.

Des. **81**, 2006, 2463-2466.

[12] T. Hemmi, N. Yanagi, G. Bansai, K. Seo, K. Takahashi, and T. Mito, Improvement of curreny decay behavior of HTS coils in persitent current operation, IEEE Trans. Appl. Supercond., **17**, 2007, 2422-2425.

[13] N. Amemiya and K. Adachi, Magnetic field generated by shielding current in high Tc superconducting coils for NMR magnets, Supercond. Sci. Technol. **21**, 2008, 095001.

[14] K. Kwasnitza and C. Widner, Strong magnetic history dependence of magnetic relaxation in high-Tc superconductors, Physica C, 184 , 1991, 341-352.

[15] Y. Iwasa, Case studies in superconducting magnets-design and operational issues, Plenum Press, New York, 1994.

[16] M. N. Wilson, Superconducting magnets, Clarendon Press, Oxford, 1983.

[17] H. Eckelmann and C. Schmidt, temperature dependence of AC-loss in Bi-2223 superconducting tapes, Physica C **372-376**, 2002, 1792-1796.

[18] L. Pust, Compariison between conventional flux creep in constant magnetic field and the effect of creep on the shape of magnetic hysteresis loops in high Tc superconductor, Supercond. Sci. Technol. **3**, 1990, 598-601.

[19] Y. Yeshurun, A.P.Malozemoff and A. Shaulov, Magnetic relaxation in

high-temperature superconductors, Rev. Modern Phys., **68**, 1996, 911-949.

[20] S. Salem-Sugui and D. Shi, Flux-creep activation energy in high-Tc superconductors, Physical Review, **46**, 1992, 6618-6621.

[21] N. Amemiya, Z. Jiang, N. Ayai and K. Hayashi, Total AC loss characteristics of high T_c superconducting tape, Physica C, **392-396**, 2003, 1083-1090.

[22] K. Yamazaki, S. Kobayashi, T. Kato, K. Ohkura, M. Ueyama, J. Fujikami, N. Ayai, E. Ueno, M. Kikuchi, K. Hayama, K. Sato and R. Hata, Development of Bi-based superconducting wire, SEI Technical Rev. , **58**, 2004, 16-22.

[23] N. Amemiya, O. Tsukamoto, M. Torii, M. Ciszek, H. Kawasaki, E. Mizushima and S. Ishii, Filament decoupling and magnetization loss of multifilamentary Bi2223 superconducting tape, IEEE Trans. Appl. Supercond., **10**, 2000, 1204-1207.

[24] K. Ohkura, K. Sato, M. Ueyama, J. Fujikami and Y. Iwasa, Generation of 24.0T at 4.2K and 23.4T at 27K with a high-temperature superconductor coil in a 22.54T background field, Appl. Phys. Lett. 13 (1995) 1923-1925.

[25] H. W. Weijers, U. P. Trociewitz, K. Marken, M. Meinesz, H. Miao, and J. Schwartz, The generation of 25.05 T using a 5.11 T $Bi_2Sr_2CaCu_2O_x$ superconducting insert magnet, Supercond. Sci. Technol. 17 (2004) 636-644.

[26] T. Kiyoshi, M. Kosuge, M. Yuyama, H. Nagai, H. Wada, H. Kitaguchi, M. Okada,

K. Tanaka, T. Wakuda, K. Ohata, and J. Sato, “Generation of 23.4 T using two Bi-2212 insert coils,” IEEE Trans. Appl. Superconduct., vol. 10, pp. 472-477, March 2000.

[27]K. R. Marken, Jr., H. Miao, M. Meinesz, B. Czabaj and S. Hong, Progress in Bi-2212 wires for high magnetic field applications, IEEE Trans. Appl. Supercond., **16**, 2006, 992-995.

[28] T. Hasegawa, T. Koizumi, Y. Hikichi, T. Nakatsu, R. M. Scanlan, N. Hirano and S. Nagaya, HTS conductors for magnets, IEEE Trans. Appl. Supercond., **12**, 2002, 1136-1140.

[29] M. Okada, Development of Bi-2212/Ag round-shaped wire and magnet application, Supercond. Sci. Tecnol, 13, 2000, 29-33.

[30] D. W. Hazelton, V. Selvamanickam, J. M. Duval, D. C. Larbalestier, W. D. Markiewitcz, H. W. Weijers, and R. L. Holtz, Recent development in 2G HTS coil technology, presented to the Appl. Super. Conf. , 3LY01 (2008).

[31] Y.Y. Xie, A. Knoll, Y. Chen, Y. Li., X. Xiong, Y. Qiao, P. Hou, J. Reeves, T. salagaj, K. Lenseth, L. Civale, B. Maiorov, Y. Iwasa, V. Solovyov, M. Suenaga, N. Cheggour, C. Clickner, J. W. Ekin, C. Weber and V. Selvamanicham, Progress in scale-up of second-generation high-temperature superconductors at SuperPower Inc., Physica C,

426-431, 2005, 849-857.

[32] M. Marchevsky, E. Zhang, Y. Y. Xie, V. Selvamanickam and G. Pethuraja, AC losses and magnetic coupling in multifilamentary coated HTS conductors and tape alloys, presented to the Appl. Super. Conf., 5MY01 (2008).

Figure Captions:

Figure 1: Numerical simulation model of the screening current-induced magnetic field. (a) Screening current is induced by the radial component of the coil magnetic field. (b) Flux penetration and screening current profile for a Bi-2223 tape during charging the coil. (c) Flux penetration and screening current profile for a Bi-2223 tape during discharging the coil.

Figure 2: Overall critical current density for a Bi-2223 tape as a function of magnetic field at 4.2K. The cases of perpendicular field application and parallel field application are compared; dashed lines shows coil load lines.

Figure 3: Hysteresis effect of the apparent magnetic field measured by a Hall sensor; the closed circles shows the field measured at the coil center, while the open circles show the field measured at the coil end. Arrows show the directions of coil charge and discharge.

Figure 4: Hysteresis effect of the screening current-induced magnetic field as a function of the coil current. Hysteresis loop moves with current along OA(0A to 100A), AB(100A to 0A), BC(0A to -100A), CD(-100A to 0A), DE(0A to 100A), and EF(100A to 0A). (a) Hysteresis effect for B_{cs}. (b) Hysteresis effect for B_{es}.

Figure 5: Flux penetration ratio (defined as $1-x_0/a$) in the coil cross section. The ratio is indicated by the color scale; red corresponds to full flux penetration, while blue no flux penetration. For the upper half, the flux is fully penetrated; for the lower half, i.e. around the coil midplane, flux penetration is limited.

Figure 6: Drift of the screening current-induced magnetic field with time: (a) B_{cs} at +100A; (b) B_{cs} at +50A ; (c) B_{cs} at -100A; (d) B_{es} at +100A; (e) B_{es} at +50A ; (f) B_{es} at -100A.

Figure 7: Remanent field drift with time. The screening current-induced magnetic field is reduced by 3 to 4G over the initial 33h and then it decays quickly with time as the temperature of the coil increases.

Figure 8: Double logarithmic plot of the remanent field (B_{esr}) vs. time. Based on the dashed line, a flux flow barrier height of 63meV is estimated.

Figure 9: $|B_{esr}(T)|/|B_{esr}(5K)|$ vs. coil temperature. The dashed line gives the $J_c(T)/J_c(5K)$ vs. temperature for the Bi-2223 tape. The remanent field disappears above 110K, corresponding to the critical temperature of Bi-2223.

Figure 10: Double logarithmic plot of $|B_{cs}|$ vs. time at +100A. The linear extrapolation of the dashed line produces a field drift rate at t =1hr of 3G/hr, which is reduced to 3 mG/hr at t =1000hr. The latter value corresponds to a rate of 10^{-8}/hr for a beyond 1GHz

NMR, sufficiently small for field frequency lock operation and high resolution NMR measurements.

Figures

Fig. 1

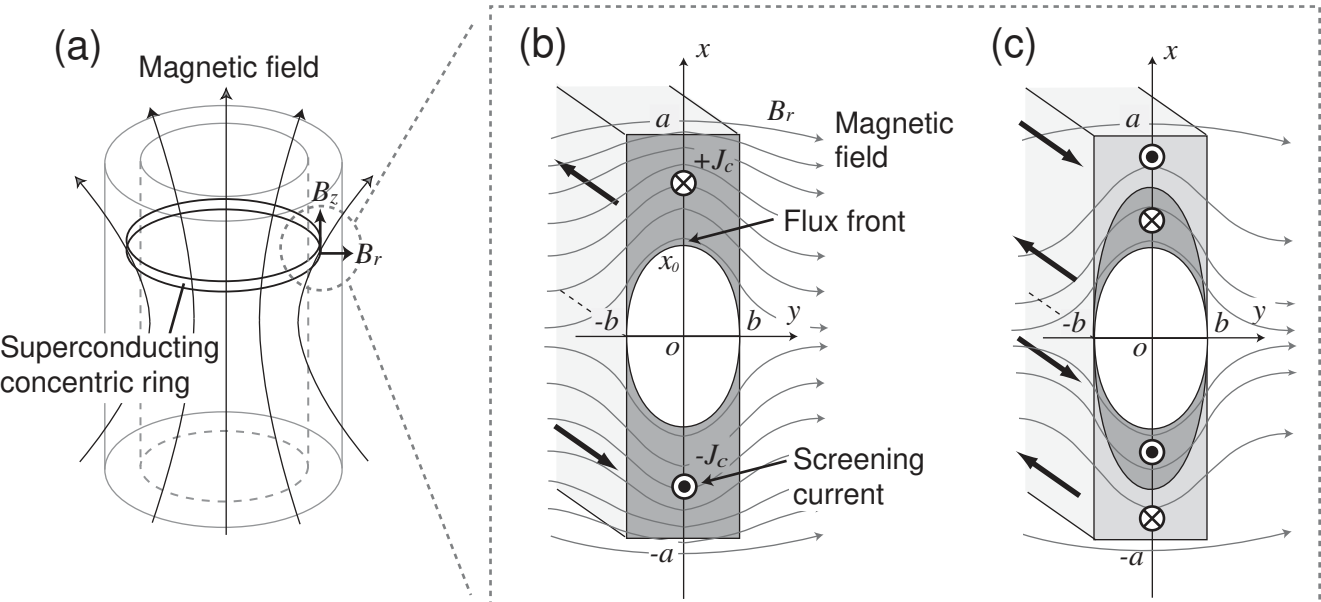

Bi-2223 double pancake coil

Cross section of the Bi-2223 tape

Fig. 2

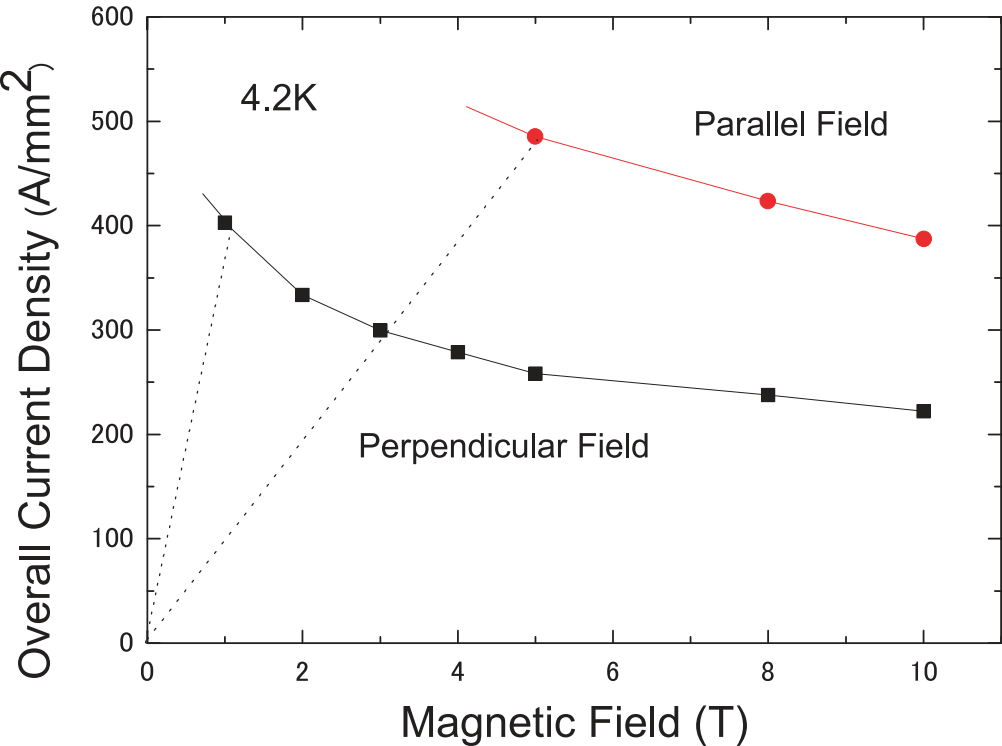
4.2K
Parallel Field
Perpendicular Field
Overall Current Density (A/mm2)
Magnetic Field (T)
600
500
400
300
200
100
0
0
2
4
6
8
10

Fig. 3

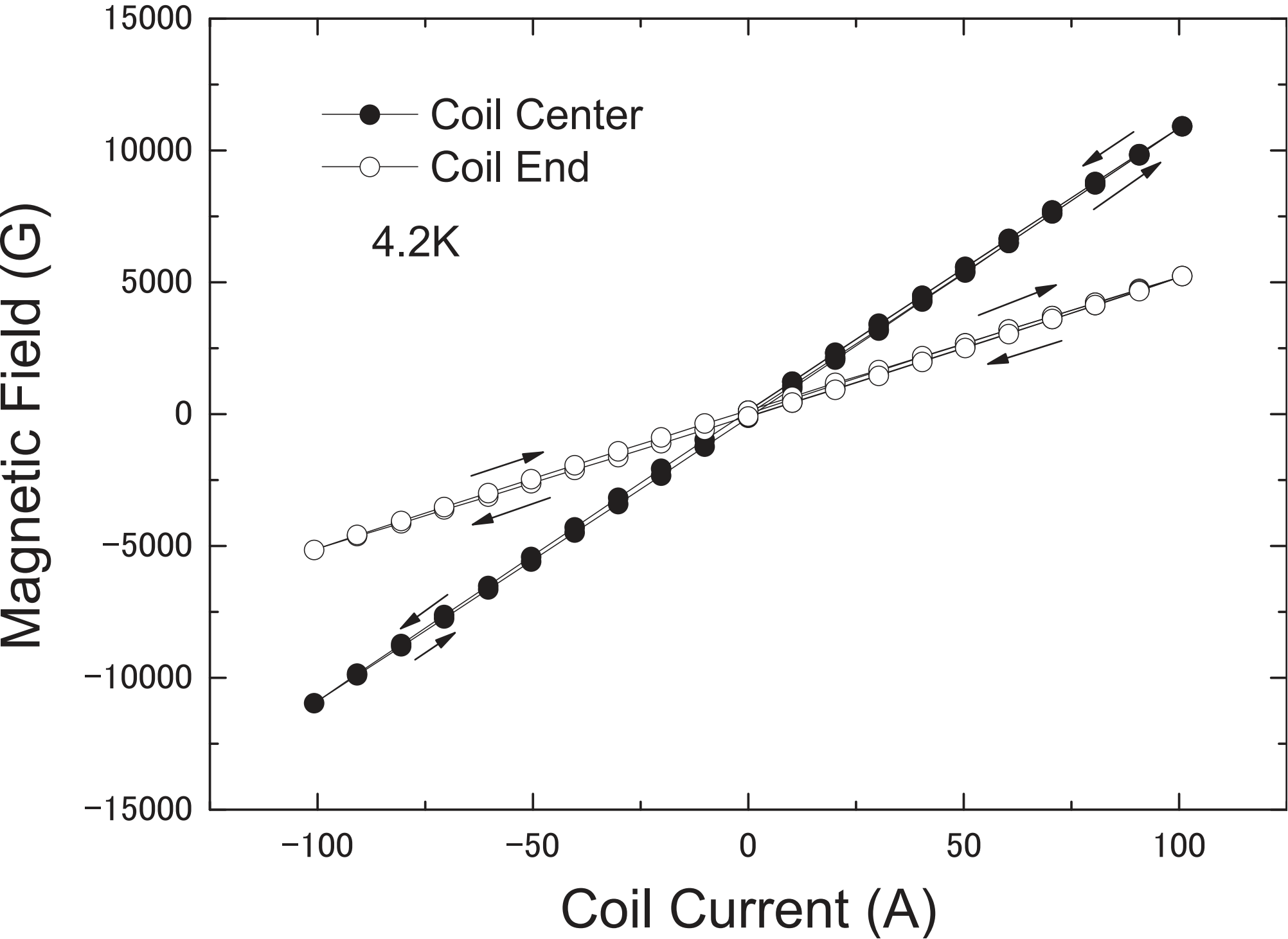
15000
10000
5000
0
−5000
−10000
−15000
−100
−50
0
50
100
Magnetic Field (G)
Coil Current (A)
Coil Center
Coil End
4.2K

Fig. 4

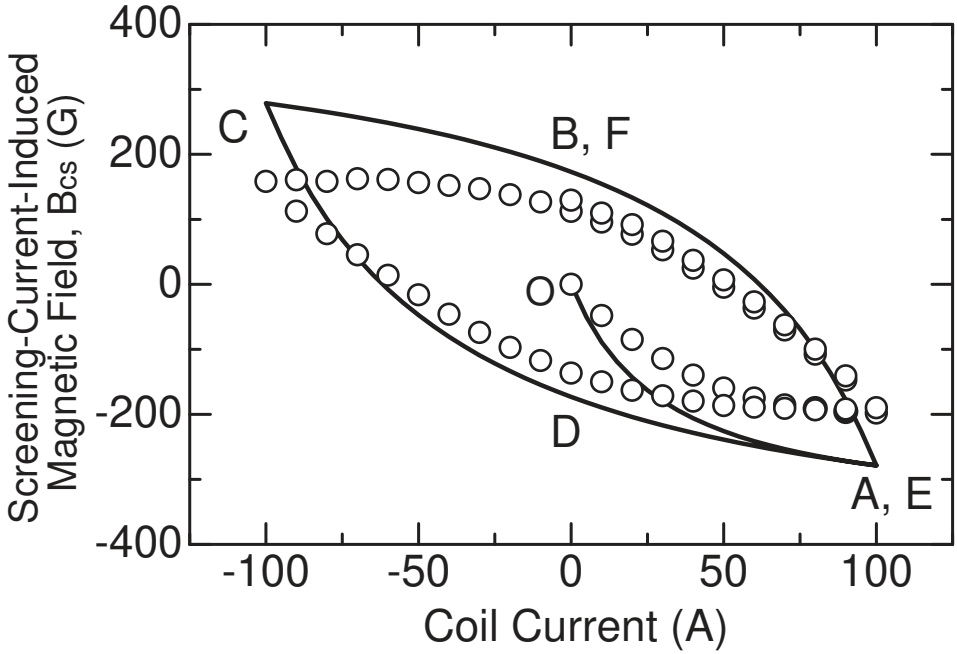
Screening-Current-Induced
Magnetic Field, Bcs (G)
400
200
0
-200
-400
-100
-50
0
50
100
Coil Current (A)
C
B, F
O
D
A, E

(a)

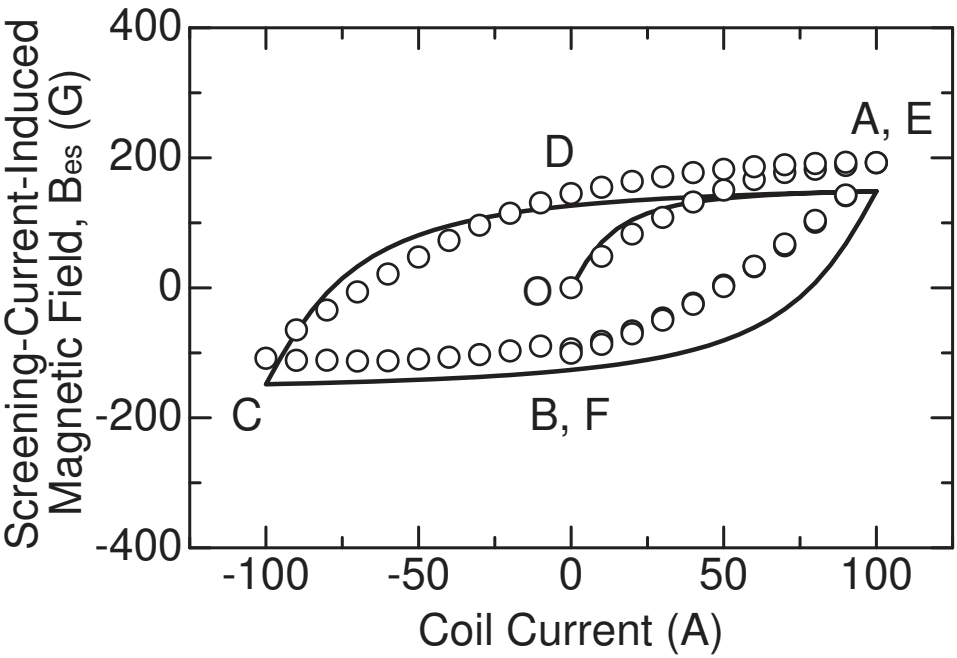
Screening-Current-Induced
Magnetic Field, Bes (G)
400
200
0
-200
-400
-100
-50
0
50
100
Coil Current (A)
A, E
D
O
C
B, F

(b)

Fig. 5

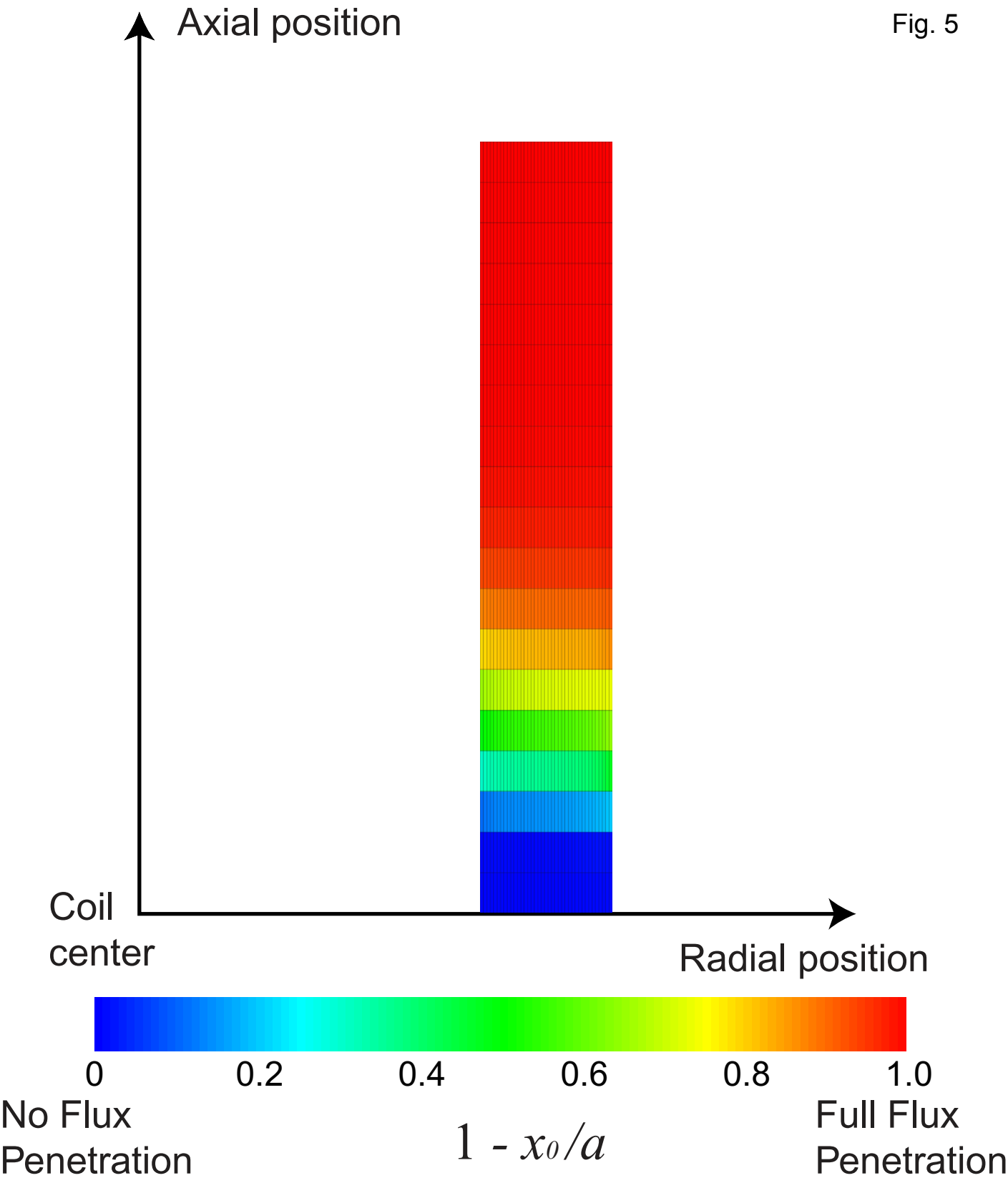
Axial position
Coil
center
Radial position
0
0.2
0.4
0.6
0.8
1.0
No Flux
Penetration
$1 - x_0/a$
Full Flux
Penetration

Fig.6

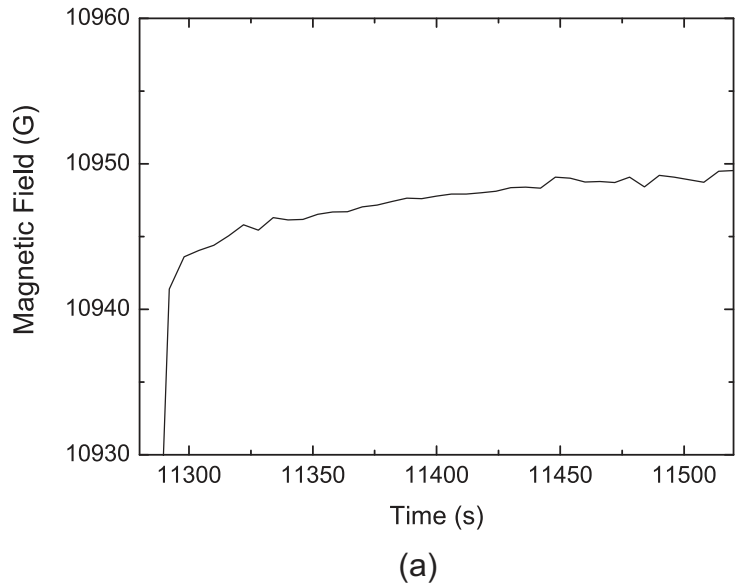
10960
10950
10940
10930
Magnetic Field (G)
11300
11350
11400
11450
11500
Time (s)

(a)

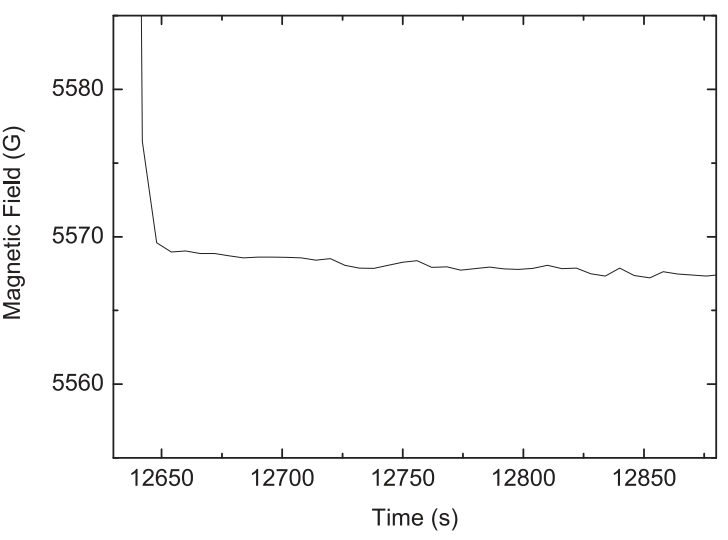
5580
5570
5560
Magnetic Field (G)
12650
12700
12750
12800
12850
Time (s)

(b)

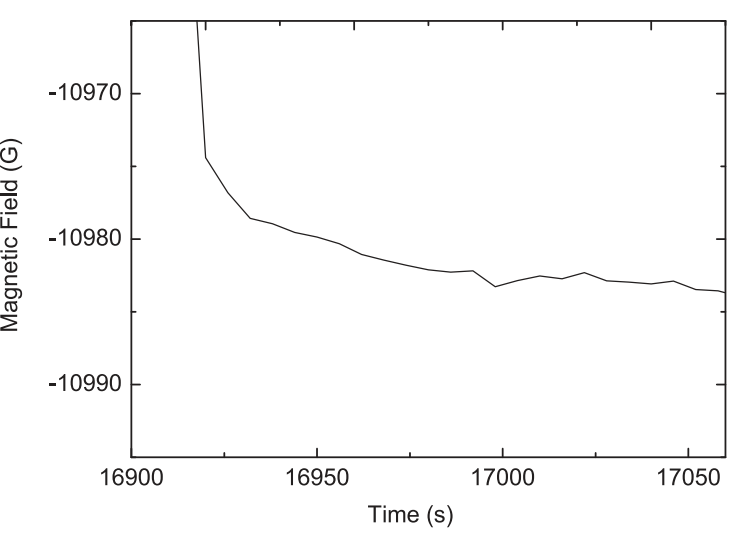
-10970
-10980
-10990
Magnetic Field (G)
16900
16950
17000
17050
Time (s)

(c)

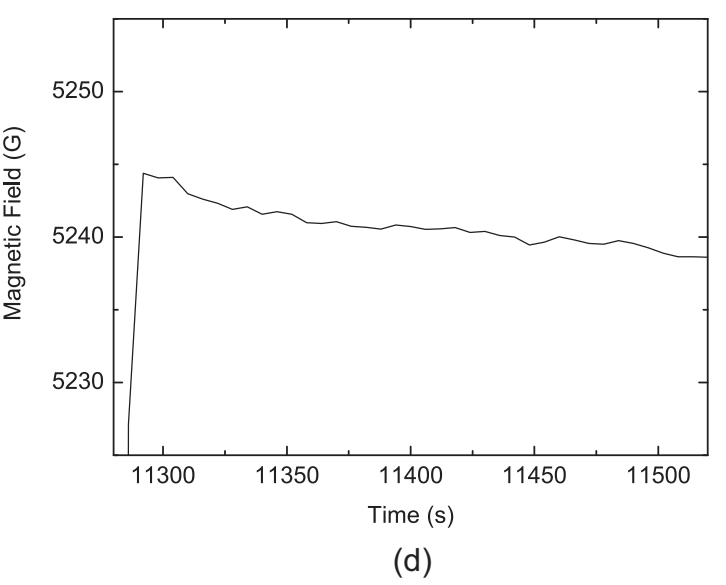
5250
5240
5230
Magnetic Field (G)
11300
11350
11400
11450
11500
Time (s)

(d)

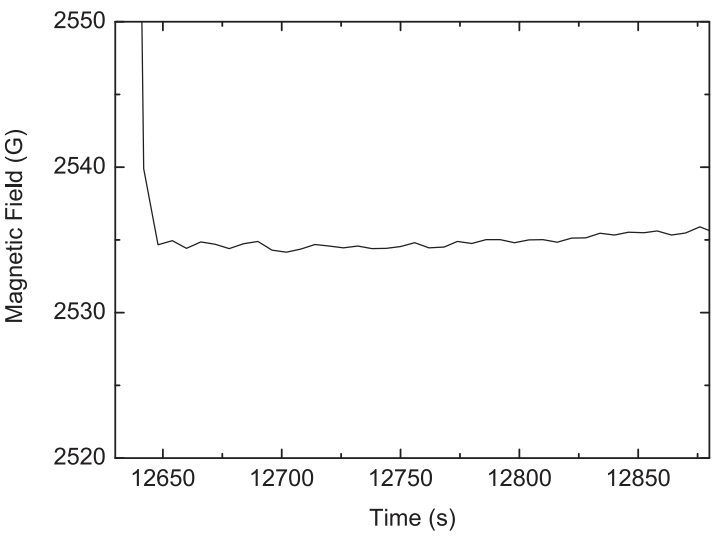
2550
2540
2530
2520
Magnetic Field (G)
12650
12700
12750
12800
12850
Time (s)

(e)

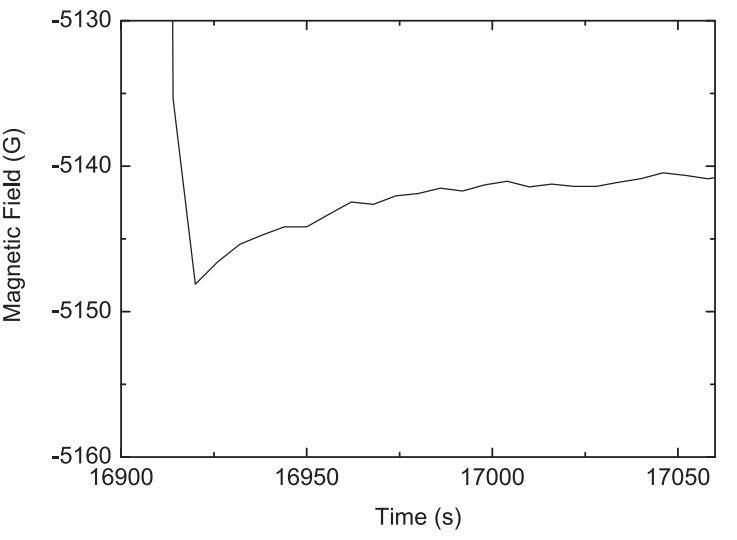
-5130
-5140
-5150
-5160
Magnetic Field (G)
16900
16950
17000
17050
Time (s)

(f)

Fig. 7

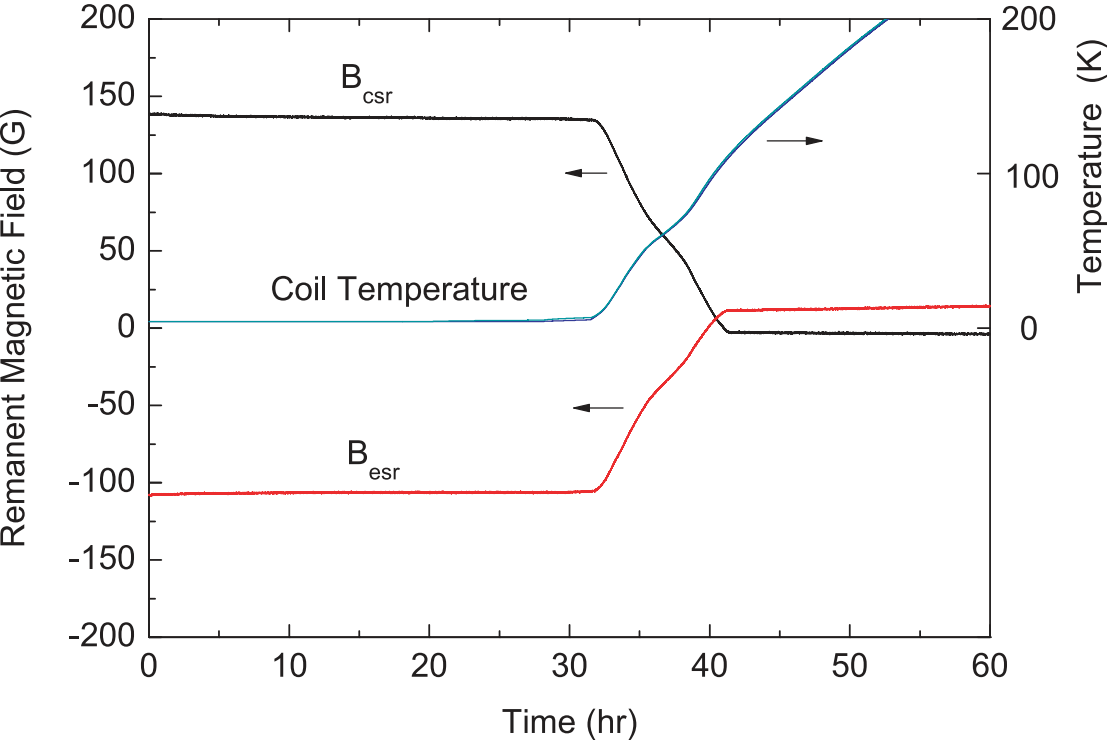
200
150
100
50
0
-50
-100
-150
-200
Remanent Magnetic Field (G)
B csr
Coil Temperature
B esr
0
10
20
30
40
50
60
Time (hr)
200
100
0
Temperature (K)

Fig. 8

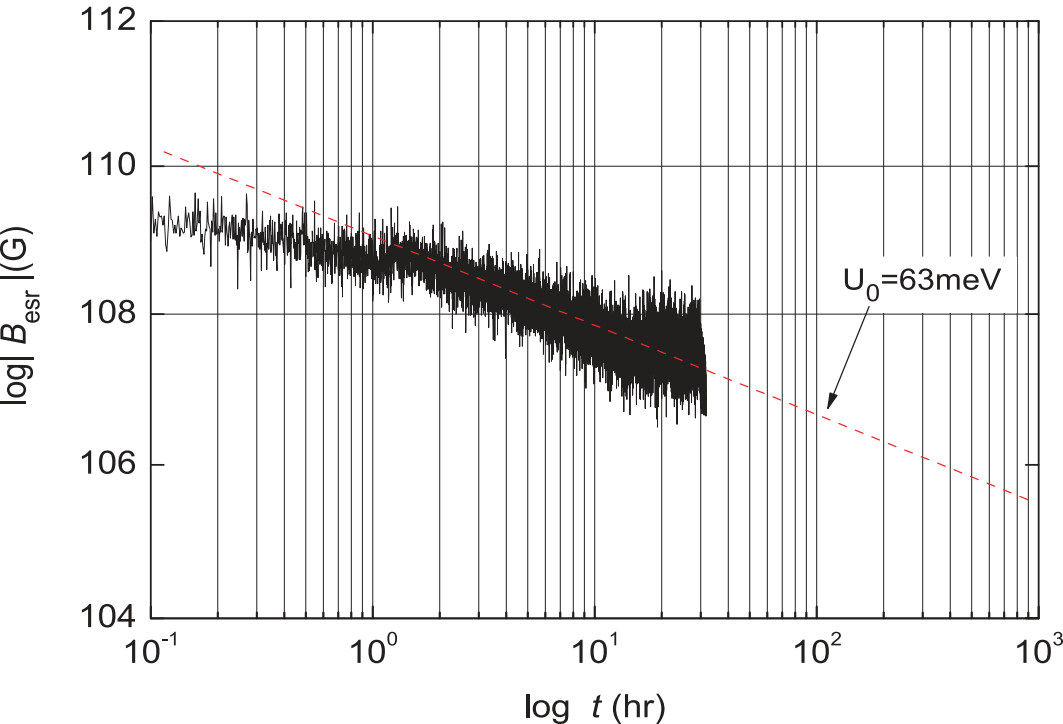
112
110
108
106
104
log| B_{esr} |(G)
10^{-1}
10^{0}
10^{1}
10^{2}
10^{3}
log t (hr)
U_0=63meV

Fig. 9

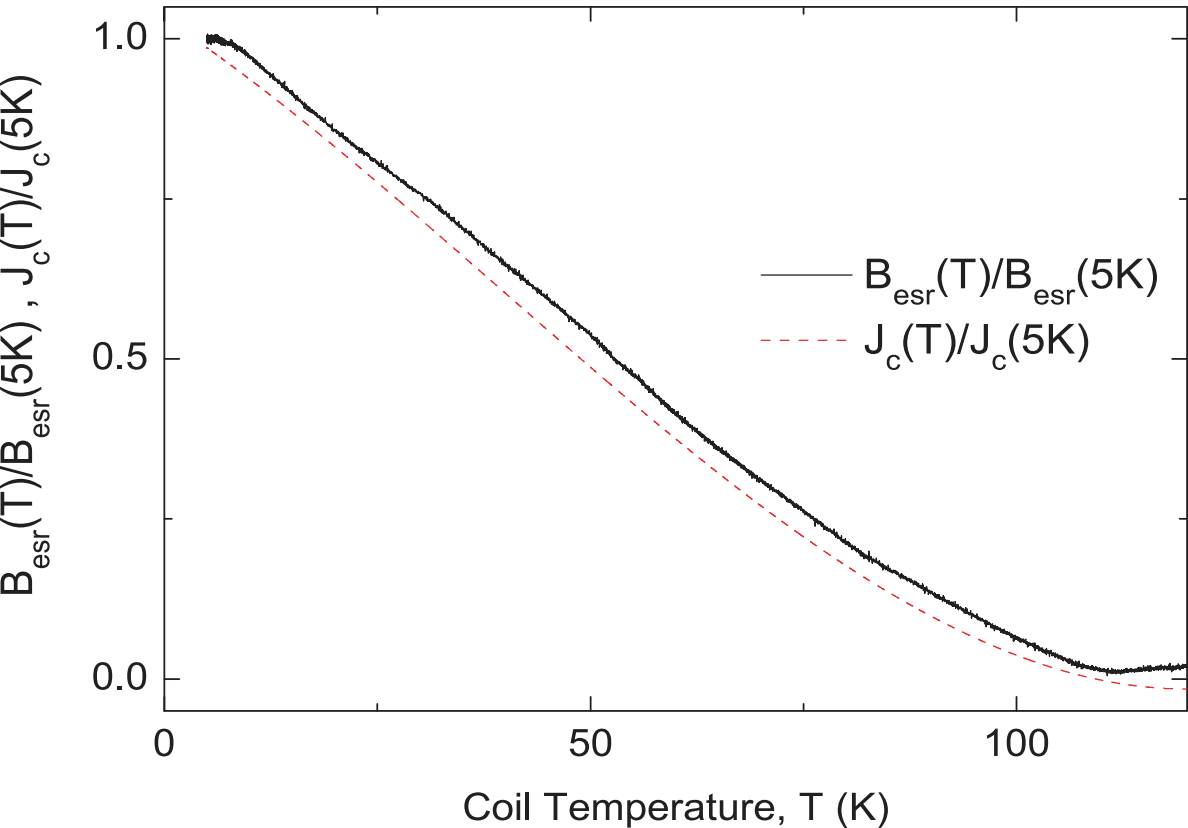
1.0
0.5
0.0
0
50
100
Coil Temperature, T (K)
B_esr(T)/B_esr(5K) , J_c(T)/J_c(5K)
B_esr(T)/B_esr(5K)
J_c(T)/J_c(5K)

Fig. 10

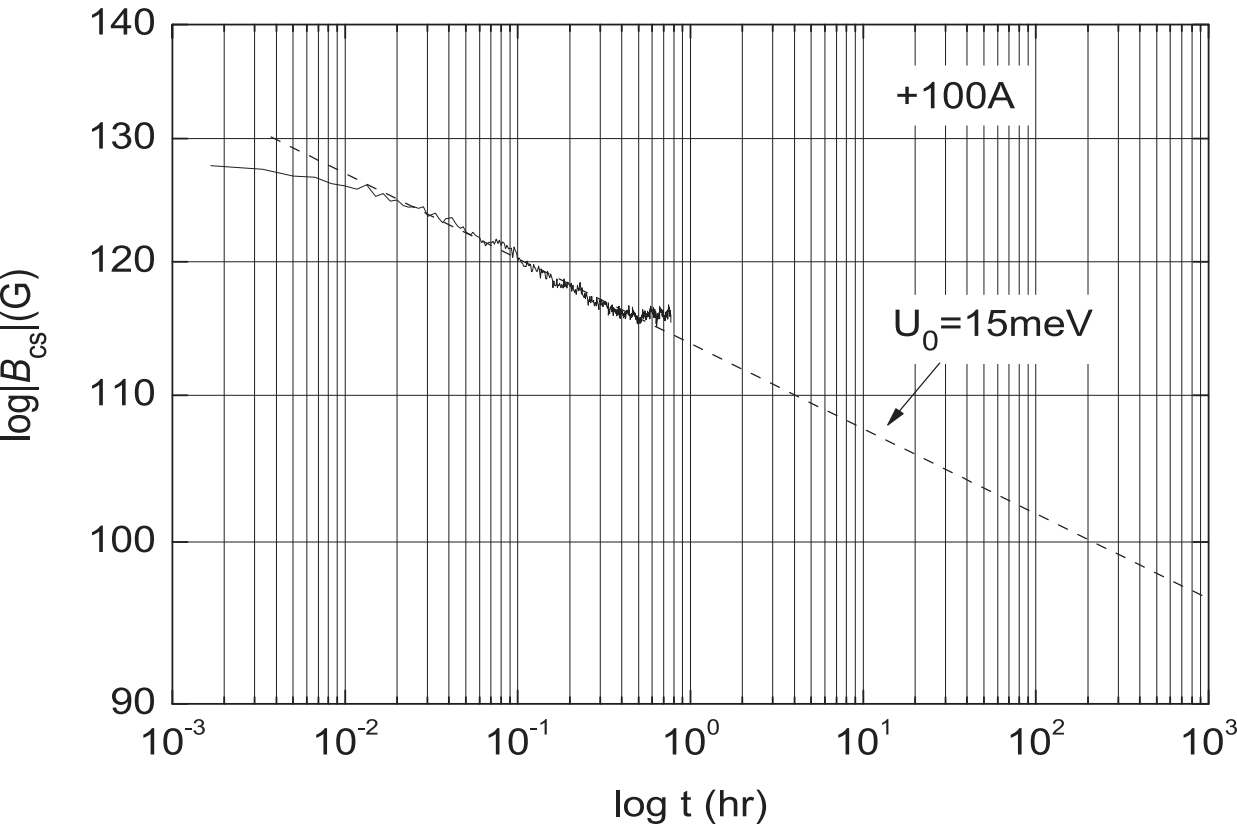
140
130
120
110
100
90
log|B_{cs}|(G)
+100A
U_0=15meV
10^{-3}
10^{-2}
10^{-1}
10^{0}
10^{1}
10^{2}
10^{3}
log t (hr)